DRAFT VERSION APRIL 30, 2018
Preprint typeset using LaTeX style emulateapj v. 01/23/15

COSMOLOGICAL PARAMETERS: AN OBSERVATIONAL DEPENDENCE ON REDSHIFT OR HOST GALAXY MASS?

J. KADOWAKI, K. LITKE, E. SPALDING[1]
[1]Steward Observatory, Department of Astronomy, University of Arizona
Draft version April 30, 2018

ABSTRACT

Though empirical support for the acceleration of the universe's expansion accumulates ever more with time, different subsamples of the data may display variations that can indicate the presence of additional systematics. One possibility is that Type Ia supernova explosion characteristics have some dependency on host galaxy properties, or that SNe Ia light curves undergo evolution through cosmic time. Here, we divide redshift-host galaxy stellar mass space, within which we re-derive the cosmological parameters Ω_M, Ω_Λ, and H_0 from a uniform dataset that covers a wide redshift range. We find that Ω_M and Ω_Λ are better constrained by the high-redshift sample, that the data subsets are in consistent agreement with a universe with a cosmological constant, and that the presence of mendacious 'grey' dust is strongly ruled out.

Keywords: Cosmology – distance scale – SNe Type Ia

1. INTRODUCTION

The discovery that the expansion of the universe is accelerating (Riess et al. (1998), Perlmutter et al. (1999), Frieman et al. (2008), and references therein) was made through a simple application of cosmological models to a small set of observational data. However, this discovery marked only the beginning of a long and continuing effort to understand the measured acceleration's full extragalactic and cosmological implications. Such an endeavor naturally requires a parallel effort to improve understanding of the underlying systematics in the available data, so as to derive stronger constraints.

The 'distance markers' that make it possible to observe the universe's expansion are Type Ia supernova (SNe Ia) explosions. These supernovae exhibit spectra bereft of hydrogen absorption lines, implying that the progenitors are bodies shorn of their stellar envelopes. These bodies are thought to be carbon-oxygen white dwarfs. However, possible models take on several different configurations, and so the exact physics that trigger the supernova explosion remain unclear (Pritchet et al. 2008; Maoz et al. 2014; Jiménez et al. 2015).

2. DATA

The data from the "Joint Light-curve Analyses" (JLA) project (Betoule, M. et al. 2014) was used to explore Type Ia supernovae in a variety of host galaxy environments with redshifts between $0.010 < z < 1.300$. A majority of the 740 spectroscopically-confirmed Type Ia supernovae compiled in the JLA data set were a part of larger concerted efforts by the Sloan Digital Sky Survey (SDSS) and the Supernova Legacy Survey (SNLS). The rest were taken from a number of low-z searches, mostly from the third release of the Whipple Observatory of the Harvard Smithsonian Center for Astrophysics (Hicken et al. 2009). The low-z data also includes data from Altavilla et al. (2004); Hamuy et al. (1996); Jha et al. (2006); Riess et al. (1999). JLA's goal to study well-calibrated supernovae light curves with accurately measured uncertainties by combining SDSS and SNLS data was largely motivated by the unprecedented number of spectroscopically-confirmed Type Ia supernovae in both surveys, as well as the complementary redshift search range.

With the suppression of each survey's unique systematic errors, the extensive JLA data has been fully inter-calibrated with well defined uncertainties, making this an attractive and reliable data set to base our study.

2.1. *Sloan Digital Sky Survey (SDSS)*

The SDSS is an ambitious, multi-year survey that has mapped one-third of the sky in *u'g'r'i'z'*-bands and has acquired five million spectra of stars, galaxies and quasars using a dedicated 2.5-meter telescope at Apache Point Observatory in New Mexico with a wide-field imager (York et al. 2000; Alam et al. 2015). The SDSS entered its second phase (SDSS-II) in 2005, which lasted for 3 years. Three surveys were conducted within SDSS-II, including the SDSS Supernova Survey, whose primary goal was to search for Type Ia supernovae over a 300 square degree field of view. The latest SDSS-II Supernova Survey data release yielded 10,258 variable and transient sources, along with their light curves (Sako et al. 2014). A few thousand of those transient sources have been identified with their host galaxies. Sources with appropriate colors and light curve slopes were targeted for spectroscopic observations at the Hobbey-Eberly Telescope (HET), the Apache Point Observatory 3.5-meter Telescope (APO), the Subaru Telescope, the Michigan-Dartmouth-MIT Observatory (MDM) 2.4-meter Hiltner Telescope, the European Southern Observatory (ESO) New Technology Telescope (NTT), the Nordic Optical Telescope (NOT), the South African Large Telescope (SALT), the William Herschel Telescope (WHT), the Telescopio Nazionale Galileo (TNG), the Keck I Telescope, and the Magellan Telescope (Frieman et al. 2007; Sako et al. 2007). In total, SDSS-II uncovered a set of 513 spectroscopically-confirmed SNe Ia (Smith et al. 2012), and SDSS-II SNe Ia comprise 374 of the 740 cataloged in the JLA (Betoule, M. et al. 2014).

2.2. *Supernova Legacy Survey (SNLS)*

The SNLS is an extensive supernova imaging and spectroscopic follow-up survey. Between 2003 and 2008, the 3.6-meter Canada-France-Hawaii Telescope monitored a 4-square-degree field split over four widely separated regions of the northern hemisphere sky, using the MegaPrime wide field imager (Astier et al. 2006). With deep observations in the *ugriz*-bands, nearly 1000 supernovae with redshifts of $0.2 < z < 1$ were detected and monitored, of which 420 were

Type Ia supernovae. The spectroscopic follow-up was conducted at several 8- to 10-meter class telescopes, including the Very Large Telescope (VLT), Gemini-North, Gemini-South, Keck-I, and Keck-II, to determine the exact nature of each supernovae candidate (Sullivan et al. 2006; Bronder et al. 2008; Balland et al. 2009). The data from the first three years of SNLS comprise 242 Type Ia supernova cataloged in the JLA.

2.3. *Additional Low-z and High-z Supernovae*

To maximize its redshift coverage, two additional data sets complete the JLA catalog. In the low redshift regime, data was acquired from the Harvard-Smithsonian Center for Astrophysics (CfA). Its third data release of photometry of 90 supernovae with redshift $z < 0.08$ was collected at the F.L. Whipple Observatory using Keplercam, Minicam, and 4Shooter2 in UBVRI-bands between 2001 and 2008. In the high redshift regime, space-based observations from the Hubble Space Telescope were acquired for 14 supernovae with redshifts $0.7 \geq z \geq 1.4$, using the wide-field mode of the Advance Camera for Surveys (ACS) and camera 2 on the Near Infrared Camera and Multi-Object Spectrometer (NICMOS).

2.4. *Joint Light-curve Analysis (JLA)*

Initiated in 2010, a collaborative effort between the SDSS-II and SNLS teams established the "Joint Light-curve Analyses" (JLA) project. The JLA's primary goals were to improve photometric calibration and uncertainty estimates in both surveys and to fully incorporate SDSS light curves as a training set for SALT2, a robust model for Type Ia supernova's time-spectral sequence.

The SDSS and SNLS use similar search strategies. Both surveys search for supernovae with a rapid, wide-field imaging with follow up spectroscopic confirmation for Type Ia candidate. The imaging phase occurs in "rolling-search" mode with single, well-characterized instruments, easing the obstacle of photometric calibration between the surveys.

The training sample for SALT2 included the previous training sample described in Guy et al. (2010) (e.g Schmidt et al. 1994; Patat et al. 1996; Hamuy et al. 2002; Benetti et al. 2004; Matheson et al. 2008; Ellis et al. 2008; Balland et al. 2009) and SDSS-II photometric data (Holtzman et al. 2008). As with the original SALT2 training sample, the SDSS-II data used only spectroscopically identified sources. SDSS-II sources with $z > 0.25$ were excluded, as there were selection biases in the sample at higher redshifts.

2.5. *Photometric Calibrations & Light Curve Recalibrations*

In both SNLS and SDSS, differential photometry was performed using "Tertiary standards," a non-variable population of stars near the Type Ia supernovae in each of the science images. All tertiary stars used varied less than a few mmag. To estimate the uncertainties of the photometric measurements, SDSS and SNLS accessed their technique by testing how well flux of test sources was recovered. SDSS used on spurious and null sources while SNLS used semi-artificial sources. Both teams recovered supernova flux down to 1.5 mmag uncertainty level.

The SDSS and SNLS samples were calibrated independently from one another, but using similar methods. The photometry of SNLS is described in Astier et al. (2013), and that of SDSS in Holtzman et al. (2008). The two samples were then calibrated jointly in Betoule et al. (2013), which improved the calibration accuracy with a revision to the effective transmission curves in MegaCam r and i bands and a correction to a non-uniformity in the SDSS photometric response.

The calibration of SNLS was further improved in the calibration of SNe light curves with respect to tertiary stars by taking into account the shape of the PSF as a function of wavelength and contamination from local background sources. SDSS-II supernova photometric calibration is described in detail in Holtzman et al. (2008), with recalibrated light curves described in Sako et al. (2014). Both samples use HST standard stars as a reference in their calibration.

Uncertainties stemming from the photometric calibration include uncertainties in the flux references, the instrument response, and the transfer between different standards. The low-z samples were calibrated with a secondary photometric standard (Smith et al. (2002); Landolt (1992)). Measurement uncertainties of BD +17 4708, a primary standard in Landolt & Uomoto (2007), are an additional, correlated source of uncertainty for the low-z sources.

3. METHODOLOGY

A recent compilation of Type Ia supernova from SDSS-II and SNLS surveys yield 740 spectroscopically confirmed supernovae with light curves (Betoule, M. et al. 2014). Supernovae from this dataset have undergone rigorous recalibrations using SALT2 light curve models. This robust procedure minimizes systemic error that arise from photometric calibration from each survey. With systematic errors between the two surveys accounted, the properties of the JLA supernovae were used to derive cosmological parameters in host galaxies with different stellar mass content at varying redshifts.

3.1. *Calculation of Distance Moduli*

We find the distance modulus, $\mu = 5\log_{10}(D_L/10\text{pc})$, for each supernova using the standardization to the supernova light curves given by Betoule, M. et al. (2014). Their analysis assumes that supernovae at all redshifts have the same intrinsic luminosity, given identical color and light-curve shape. The distance modulus is linearly modeled as

$$\mu = m_B^\star - (M_B - \alpha \times X_1 + \beta \times C)\,. \tag{1}$$

$m_B^\star$ is the observed rest-frame B-band peak magnitude. X_1 describes the time-stretch of the light curve, and C describes the color of the supernova when it is at its maximum brightness. α and β were determined by Betoule, M. et al. (2014) alongside the cosmological parameters, as was M_B. M_B is the absolute magnitude of the supernovae. Both M_B and β depend on the host galaxy (see Sullivan et al. 2011; Johansson et al. 2013). In particular, the color-stretch has been found to be higher in galaxies with higher star formation rates (Conley et al. 2011). The effect of the host galaxy property on the supernova absolute magnitude is corrected for by assuming the absolute magnitude depends on the mass of the host galaxy:

$$M_B = \begin{cases} M_B^1, & M_{stellar} < 10^{10} M_\odot \\ M_B^1 + \Delta_M, & M_{stellar} \geq 10^{10} M_\odot. \end{cases} \tag{2}$$

The correction is made as a function of stellar mass (as opposed to metallicity, star formation rates, star formation history, or other host galaxy properties) because the stellar mass is the most well-constrained host-galaxy property (Conley et al. 2011).

For M_B^1, Δ_M, α, and β, we use the best-fit parameters for the JLA sample found by Betoule, M. et al. (2014). This model assumed a flat universe with a cosmological constant and used

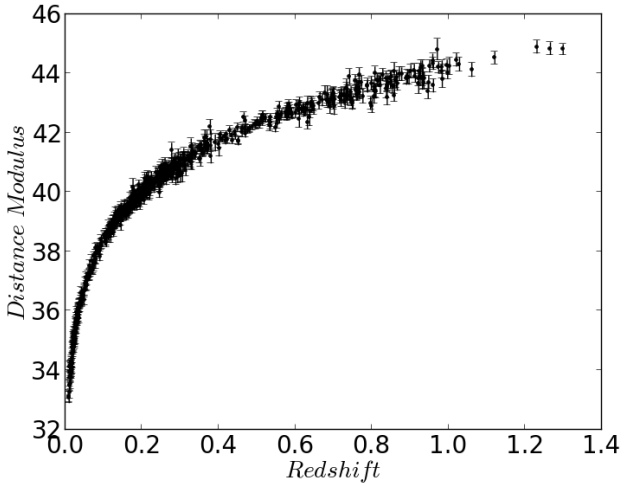

Figure 1. Distance modulus vs redshift for the supernovae in our sample. Distance moduli were calculated using Equation 1.

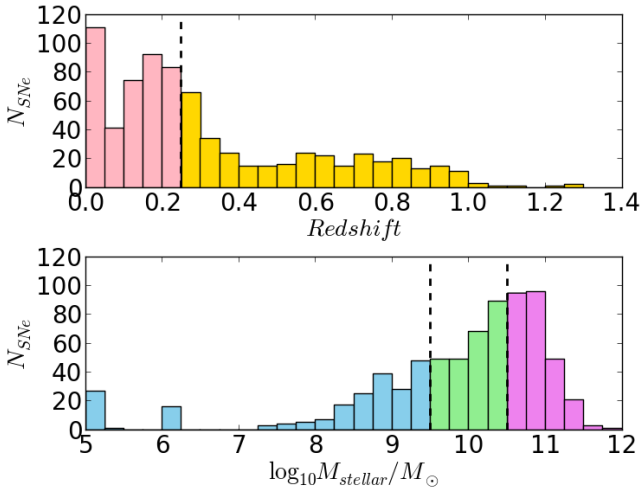

Figure 2. Top: histogram of supernova redshifts. Pink bins show the low-redshift sample, and gold bins show the high-redshift sample. Bottom: histogram of supernova host galaxy stellar masses. Blue is the low-mass sample, green the mid-mass sample, and purple the high-mass sample. Lines delineate the redshift and stellar mass divisions used.

only Type Ia SNe. The fit to the JLA sample was chosen because this sample was used to train the SALT2 data and provided the basis for the SNe light curve parameterization. This fit were also used because it includes only SNe Ia data, as does our own analysis. The best-fit parameters used were $M_B^1 = -19.05 \pm 0.02$, $\Delta_M = -0.70 \pm 0.023$, $\alpha = 0.141 \pm 0.006$, and $\beta = 3.101 \pm 0.075$. The values for M_B^1, α, and β determined for different models and data sets by Betoule, M. et al. (2014) were generally similar. The exceptions were the fits for α that included the data from Conley et al. (2011) because this sample used a different parameterization of the time-stretch. Δ_M showed the most variation between different data sets and models, but this parameter was only a simple correction to account for host galaxy properties and likely does not fully cover the supernova absolute brightness dependence on host galaxy mass.

Errors for the distance moduli were calculated using

$$\sigma_\mu = \left[\sigma^2_{m_b^*} + \sigma^2_{M_b} + \alpha^2\sigma^2_{X_1} + X_1^2\sigma^2_\alpha + \beta^2\sigma^2_C + C^2\sigma^2_\beta\right]^{1/2}. \quad (3)$$

For supernovae in galaxies with $M_{stellar} \geq 10^{10}$ $M_\odot$, $\sigma^2_{M_b} = \sigma^2_{M_B^1} + \sigma^2_{\Delta_M}$ and $\sigma^2_{M_b} = \sigma^2_{M_B^1}$ for $M_{stellar} < 10^{10}$ $M_\odot$.

Figure 1 shows the calculated distance moduli as a function of redshift.

3.2. *Redshift & Stellar Mass subsamples*

In this analysis, we consider both the effects of redshift and host galaxy properties on the cosmological parameters. For host galaxy properties, we look at galaxies with different stellar masses. We divide the data into two redshift subsamples and three stellar mass subsamples so that the six subsamples have approximately the same number of supernovae in each subsample. This division allows us to avoid very small sample sizes.

The supernovae are divided in redshift at $z = 0.25$. The low-redshift subsample includes just over half of the total 740 SNe sample ($z = 0.23$ divides the sample evenly by redshift, but does not allow for evenly distributed mass subsamples). The SDSS-II data excluded SNe with $z > 0.25$ due to selection biases; our redshift cut is consistent with the SDSS-II cut. Betoule, M. et al. (2014) defined their low-redshift sample as $z < 0.1$ This redshift cut was considered but not used in order to avoid small sample sizes. The entire sample includes

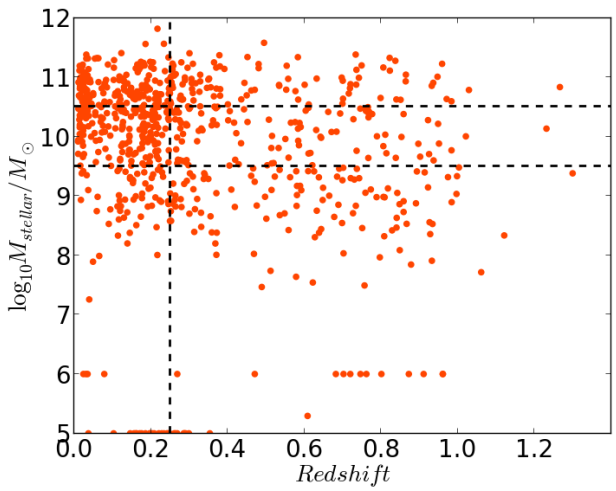

Figure 3. Redshift and stellar mass subsamples of Type Ia SNe data.

supernovae at redshift $0.01006 \leq z \leq 1.299106$. The top panel of Figure 2 shows a histogram of the redshifts in the sample.

The supernovae are also divided into stellar mass subsamples with cuts at $M_{stellar} = 10^{9.5}$ $M_\odot$ and $M_{stellar} = 10^{10.5}$ $M_\odot$. The middle mass subsample includes supernovae with and without the correction to M_B to account for higher mass galaxies. The supernova host galaxy stellar masses range from $10^{5.0}$ $M_\odot \leq M_{stellar} \leq 10^{11.817}$ $M_\odot$. A histogram of host galaxy stellar masses is shown in the bottom panel of Figure 2.

Figure 3 shows the final redshift and stellar mass subsamples. The total number of supernovae in each subsample is listed in Table 1.

3.3. *Statistical Derivation of Cosmological Parameters*

3.3.1. *Predicted Distances to Type Ia Supernova*

By definition, empirical measurements of a supernova luminosity $\mathcal{L}$ correspond to a luminosity distance

$$D_L \equiv \left(\frac{\mathcal{L}}{4\pi\mathcal{F}}\right)^{1/2} \quad (4)$$

Table 1
Number of galaxies in each redshift-stellar mass subsample.

Redshift	M_* ($M_\odot$)	N_{SNe}
$z < 0.25$	$M_* < 10^{9.5}$	82
$z < 0.25$	$10^{9.5} < M_* \leq 10^{10.5}$	154
$z < 0.25$	$M_* \geq 10^{10.5}$	165
$z \geq 0.25$	$M_* < 10^{9.5}$	138
$z \geq 0.25$	$10^{9.5} < M_* \leq 10^{10.5}$	101
$z \geq 0.25$	$M_* \leq 10^{10.5}$	100
Total		**740**

where $\mathcal{F}$ is the flux at the position of the observer. In an Einsteinian, general relativistic universe, it is expected to behave as

$$D_L = H_0^{-1} c(1+z)|\Omega_k|^{-1/2} \sin^* \left\{ |\Omega_k|^{1/2} \times \int_0^z dz \left[(1+z)^2(1+\Omega_M z) - z(2+z)\Omega_\Lambda\right]^{-1/2} \right\} \quad (5)$$

where H_0 is the Hubble constant, Ω_M is the mass density, cosmological constant Ω_Λ is the vacuum energy density, and $\Omega_k \equiv 1-\Omega_M-\Omega_\Lambda$ describes the curvature of the universe (e.g., Carroll et al. (1992); Riess et al. (1998); Leibundgut (2001)). The $\sin^*$ term is dependent on the curvature, where

$$\sin^* = \begin{cases} \sin & \Omega_k < 1 \\ \sinh & \Omega_k \geq 1. \end{cases}$$

which correspond to negative and positive curvature universes, respectively. From the luminosity distance, the distance modulus is

$$\mu \equiv 5\log_{10}(D_L/10\text{pc}) \quad (6)$$

3.3.2. *Observed Distances to Type IA Supernovae*

Type Ia supernovae are thought to be an homogeneous class due to fixed progenitor mass set by the Chandrasekhar limit. Yet, these supernovae are imperfect standard candles. Large intrinsic dispersion of Type Ia supernova's peak luminosity is observed when estimating their distances with the Tully-Fisher relation or with fluctuations in surface brightness of their host galaxy (Phillips 1993). The adjusted luminosity with respect to their decay rate, using a light curve slope parameter b, eliminates much of this dispersion (Phillips 1993; Hamuy et al. 1995; Hamuy et al. 1996). Incorporating a color correction parameter R removes virtually all dispersion (Tripp 1998).

A more complete description of the observed moduli is described in Section 3.1. The Appendix describes the procedure used to fit for different cosmological models using Bayes' theorem.

3.3.3. *Fitting and Marginalization over Cosmological Parameters*

The observed and predicted ΛCDM distance moduli yielded χ^2 values for each supernova in the sample. Once the supernovae were divided into two redshift and three host galaxy stellar mass subsamples, best estimates for the Hubble constant H_0, mass density Ω_M, and dark energy density Ω_Λ were derived. This was achieved using a Bayesian approach further detailed in Section 4, the Appendix, and Riess et al. 1998. The basic approach considers a mass density of $0 \leq \Omega_M < 2.5$, a dark energy density of $-1 \leq \Omega_\Lambda < 3$, and a Hubble constant of $60 \leq H_0 \leq 80\,\text{km s}^{-1}\cdot\text{Mpc}^{-1}$ with uniform priors across the defined parameter space. We considered a wide parameter space with uniform priors to allow for our best fit cosmological parameters to remain unbiased to previous measurements on data from other surveys. The lower bound of the mass density was set to $\Omega_M = 0$, since a universe with $\Omega_M < 0$ would not correspond to any physical reality. The bounds on the remaining parameters were largely motivated by previous works to ensure the parameter space reasonably encompassed the probability distribution function for the high-redshift supernovae sample. Additionally, regions in parameter space corresponding to a bouncing or rebounding universe were omitted from the analysis. Since the regions producing a bouncing or rebounding universe varied with H_0, the omitted (Ω_M, Ω_Λ) parameter space were individually computed at every H_0. χ^2 values for the distance moduli were considered at every 0.025 steps in Ω_M, 0.04 steps in Ω_Λ, and 0.1 steps in H_0, yielding a resolution probability density functions for each redshift-stellar mass subsample. Assuming distance moduli for every supernova are independent with Gaussian errors, the χ^2 values are converted to probability densities. An example of a normalized probability density function is shown in Figures 7 and 8 for supernovae with host galaxy stellar mass $10^{9.5} < M_* < 10^{10.5}\,\text{km s}^{-1}\cdot\text{Mpc}^{-1}$ with redshifts $z < 0.25$ and $z \geq 0.25$.

Marginalizing over H_0 yielded probability density functions for (Ω_M, Ω_Λ) in each redshift-stellar mass subsample. Confidence intervals and best-fit parameters were subsequently derived for Ω_M, Ω_Λ, and H_0.

4. RESULTS

As an example, the evolution of the (Ω_M, Ω_Λ) probability distribution across selected H_0 values is shown in Figures 7 and 8 for supernovae with host galaxy stellar mass $10^{9.5} < M_* < 10^{10.5}\,\text{km s}^{-1}\cdot\text{Mpc}^{-1}$. The colors indicate the probability for the set of cosmological parameters (Ω_M, Ω_Λ, H_0) to characterize the universe based on the JLA dataset. The solid white lines indicate the divide between an open and closed universe and one which expands to infinity or recollapes. The dashed lines mark the values for deceleration parameters $q_0 = -0.5, 0, 0.5$. The white areas correspond to regions in parameter space which yield an nonphysical universe.

By integrating over H_0, we obtain the marginalized probability distribution function for (Ω_M, Ω_Λ) in every redshift-stellar mass subsample as denoted in Figure 4. Even by eye, Ω_M and Ω_Λ are not well constrained for low-redshift supernovae. Figure 5 shows the marginalized distributions for all three cosmological parameters with their respective 1- and 2-σ confidence intervals in each subsample. Table 2 lists the best-fit parameters and their $1-\sigma$ errors.

In the low-redshift regime, the stellar mass of the host galaxy appears to affect the shape of the Ω_M and Ω_Λ profiles and the observed width of the H_0 distribution. This is simply an artificial result due to the boundaries placed on the considered parameter space. The chosen boundaries were motivated to exclude areas which yielded cosmological parameters corresponding to a nonphysical universe and by previous work which simultaneously analyzed low- and high-redshift supernovae. The considered parameter space encapsulates the high-redshift probability distribution, but not the low-redshift results. We therefore assigned the probability of an cosmological parameter which fell outside of the boundaries to be 0. The profiles for all three cosmological parameters were affected by this boundary treatment. The shape and width were dominantly affected by where the peak of the probability dis-

Table 2
Calculated Cosmological Parameters

z	$M_*/M_\odot$	Ω_Λ	Ω_M	$H_0/(kms^{-1}Mpc^{-1})$
< 0.25	$< 10^{9.5}$	$1.22^{+0.69}_{-0.81}$	$1.41^{+0.76}_{-0.91}$	$68.7^{+1.8}_{-1.8}$
< 0.25	$10^{9.5}$ to $10^{10.5}$	$1.95^{+0.57}_{-0.69}$	$1.54^{+0.68}_{-0.93}$	$72.0^{+1.1}_{-1.1}$
< 0.25	$\geq 10^{10.5}$	$1.67^{+0.65}_{-0.65}$	$1.26^{+0.83}_{-0.83}$	$70.6^{+0.9}_{-0.9}$
≥ 0.25	$< 10^{9.5}$	$0.37^{+0.48}_{-0.53}$	$0.23^{+0.18}_{-0.15}$	$67.3^{+3.6}_{-3.4}$
≥ 0.25	$10^{9.5}$ to $10^{10.5}$	$0.74^{+0.44}_{-0.48}$	$0.25^{+0.18}_{-0.18}$	$70.3^{+3.6}_{-3.5}$
≥ 0.25	$\geq 10^{10.5}$	$0.49^{+0.44}_{-0.44}$	$0.18^{+0.15}_{-0.13}$	$69.0^{+3.4}_{-3.5}$

tribution falls in the parameter space.

The Hubble constant H_0 is better constrained with low-redshift supernovae. This phenomenon is due our abilities to measure distances and magnitudes of nearby, low-redshift supernovae with higher precision. In contrast, both Ω_M and Ω_Λ are better constrained using high-redshift supernovae. The stark contrast between the profiles of Ω_M and Ω_Λ in low- and high-redshift can be partially attributed to the wider redshift coverage ($0.25 \leq z < 1.3$) and to the highest redshift supernovae occurring in a matter-dominated era.

5. DISCUSSION

5.1. *Consistency with a Cosmological Constant or Pernicious Dust?*

An Akaike Information Criterion (AIC) and Bayesian Information Criterion (BIC) test were applied to the data so as to determine whether our results were consistent with a universe with a zero or nonzero cosmological constant. The AIC is a test that checks for the fit of a dataset to a model and penalizes the number of model parameters so as to avoid overfitting (Akaike 1974). Using a chi-squared value of a model fit, it is calculated as

$$AIC = \chi^2 + 2k + \frac{2k(k+1)}{N-k-1} \tag{7}$$

where k is the number of fitted parameters (which varies between 2 and 3, depending on whether the universe has a cosmological constant or not), and N is the number of data points in the appropriate $z-M$ subsample. The best model is the one with the smallest AIC.

The BIC (Schwarz et al. 1978) is a statistic used to make model comparisons based on Bayesian reasoning, where the model priors are poorly-constrained. Using χ^2, we have

$$BIC = \chi^2 + kln(N) \tag{8}$$

where the second term rapidly increases with the number of model parameters.

We find that each subsample of data very strongly favors a universe with $\Omega_\Lambda \neq 0$ for most values of Ω_M, though the disagreement is only 'strong' at the lowest values of Ω_M (Fig.6). This would imply that hidden systematics, such as variations of a a scenario involving self-regenerating 'grey' dust, would have to mimic cosmic acceleration to a very high degree indeed.

In particular, such dust would have to exist and self-regenerate out to beyond $z > 0.25$, or equivalently, beyond a luminosity distance of ~ 1.3 Gpc, or a comoving volume of 4.4 Gpc^3 in a flat universe (Wright 2006). These distance scales are extraordinary, corresponding to sizes larger than the coherent large-scale structure of matter expected to be typically a few hundred Mpc in size from simulations, and the largest observed structures of less than 500 Mpc (Park et al. 2012). There is scarcely any conceivable mechanism that could continually and uniformly spew nucleosynthetic products from galactic centers into the IGM in such a manner.

5.2. *The Hubble Parameter*

As seen in Figures 7 and 8, the value of the Hubble constant H_0 greatly affects the probability distribution for (Ω_M, Ω_Λ). In the low-redshift regime, H_0 is better constrained due to Malmquist bias. This leads to a concencration of the probability distribution at low-redshifts in frames with Hubble constant of $70 \leq H_0 \leq 74\,\mathrm{Mpc \cdot km^{-1}\,s}$. In contrast, the high-redshift distribution is spread over all frames ($63 \leq H_0 \leq 78\,\mathrm{Mpc \cdot km^{-1}\,s}$).

As discussed in Section 4, H_0 appears to be better constrained in higher mass subsamples. However, this is simply an artifact arising from boundary cuts and from the peak position of the distribution function relative to these boundaries. Therefore, a conclusion about a host galaxy's stellar mass content cannot be made for the low-redshift regime. Negligible differences are observed in the high-redshift regime, suggesting that the host galaxy's stellar mass does not play a role on the measurement of H_0.

The location of the probability distribution peak progressively shifts toward larger Ω_Λ and Ω_M values for larger H_0. This result can be attributed to the greater energy densities required to increase the rate of the universe's expansion.

5.3. *Effects of Redshift and Stellar Mass*

Due to the bias introduced to the (Ω_M, Ω_Λ) probability distribution for the low-redshift supernova by the selected boundaries in parameter space, it is difficult to draw specific conclusions about the effects of stellar mass on Ω_M and Ω_Λ in the low-redshift regime. However, to first order, best-fit values for Ω_M and Ω_Λ across all stellar mass ranges are consistent. In the high-redshift sample, there is no trend for the best-fit value for Ω_Λ. Whether an inverse correlation exists between Ω_M and host galaxy stellar mass is hard to determine. If this correlation is real, variations in supernovae and host galaxy properties attributed to metallicity and stellar age must be examined.

Despite our limited abilities to draw conclusions regarding the effects of host galaxy's stellar mass content, the redshift of the supernovae have a large impact on Ω_Λ and Ω_M. Notably, The 95% confidence interval for Ω_M hardly rules out any parameter space from $0 \leq \Omega_M < 2.5$ for low-redshift supernovae. Yet, a sharp peak is observed for Ω_M between 0.18 - 0.25 in the high-redshift dataset. A similar effect is observed with Ω_Λ to a lesser extent.

5.4. *Corrections for Host Galaxy Parameters*

Sullivan et al. (2010) originally split their SN sample at $10^{10}\ M_\odot$ in order to have samples of equal size. They found that SNe in more massive hosts were intrinsically brighter, and that this trend is present wherever the host galaxy stellar mass subsamples are divided. We would expect the three host galaxy stellar mass subsamples used in our analysis to have different intrinsic brightnesses. However, as a simple model we used the two-step model and values modeled by Betoule, M. et al. (2014). The absolute magnitude of the supernovae would likely be better fit by a three-step function, rather than by two steps, or ideally with a more continuous stellar mass-intrinsic luminosity relation.

A more accurate, three-step model would require additional fitting; determining the necessary corrections to the

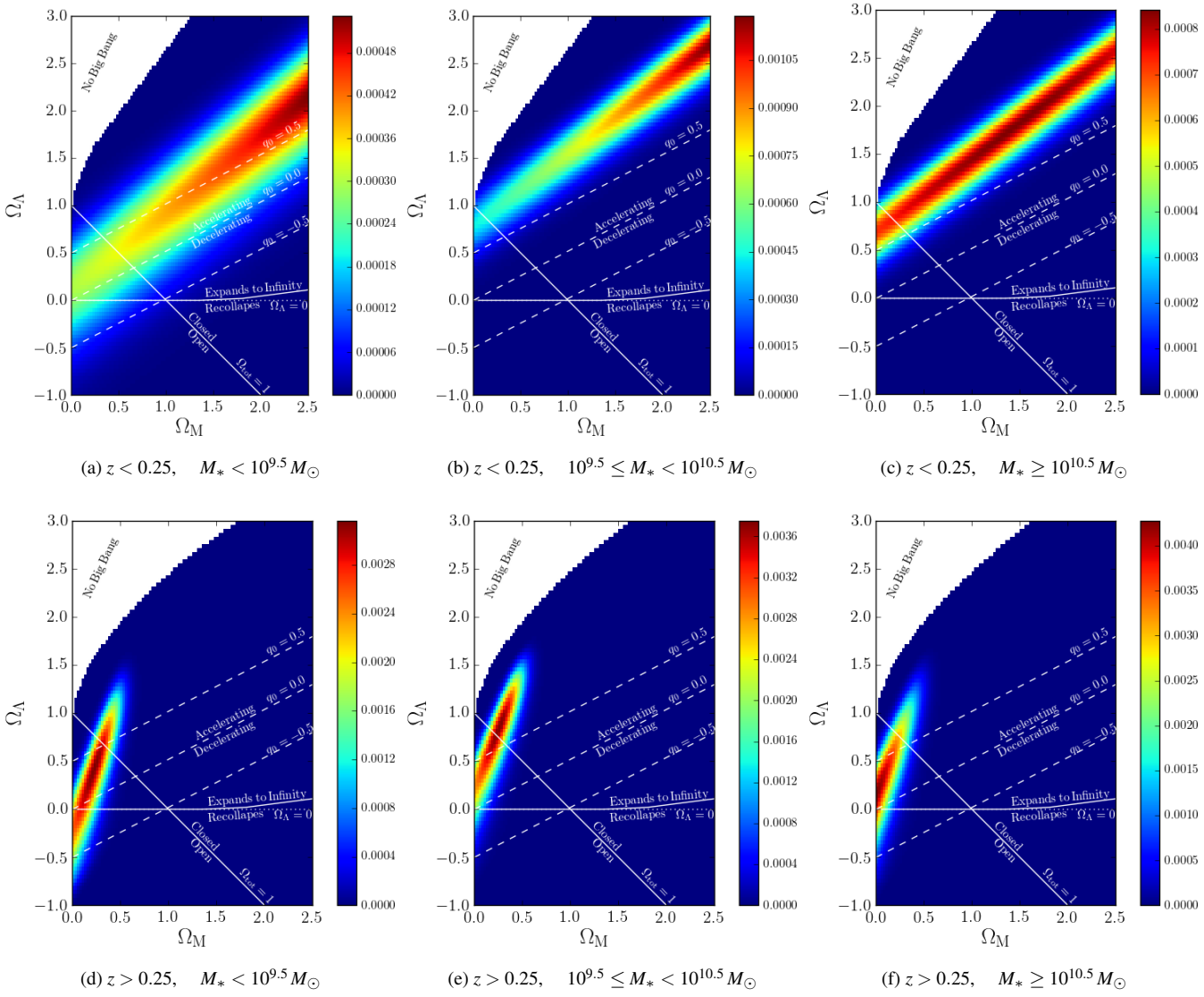

(a) $z < 0.25$, $M_* < 10^{9.5}\,M_\odot$ (b) $z < 0.25$, $10^{9.5} \leq M_* < 10^{10.5}\,M_\odot$ (c) $z < 0.25$, $M_* \geq 10^{10.5}\,M_\odot$

(d) $z > 0.25$, $M_* < 10^{9.5}\,M_\odot$ (e) $z > 0.25$, $10^{9.5} \leq M_* < 10^{10.5}\,M_\odot$ (f) $z > 0.25$, $M_* \geq 10^{10.5}\,M_\odot$

Figure 4. The marginalized probability density functions for $(\Omega_M, \Omega_\Lambda)$ for all redshift-stellar mass subsamples. The solid white lines indicate the divide between an open and closed universe and one which expands to infinity or recollapes. The dashed lines mark the values for deceleration parameters $q_0 = -0.5, 0, 0.5$. The white areas correspond to regions in parameter space which yield an nonphysical universe.

light curves due to host galaxy properties is not trivial. Any changes in the intrinsic properties of SNe as a function of redshift are difficult to study, as corrections to the distance moduli for an evolution in SNe mechanics could also be accounted for using a different cosmological model. Other studies (for example, Sullivan et al. (2010)) have worked under the hypothesis that changes in the intrinsic properties of SNe Ia light curves are, on average, reflected in the properties of their host galaxies. Studying the evolution of galaxies in more detail, and the effects of different host galaxy properties on SNe Ia light curves, would allow future studies to better correct the light curves for host galaxy properties.

Conley et al. (2011) noted that the stellar mass of the host galaxy was used to correct for host galaxy properties because it is the most well constrained property of the host galaxies. However, stellar mass is not the only host galaxy property that can affect SNe properties. Other things to consider include the specific star formation rate, the age of the stellar population, and the metallicity of the galaxy.

Sullivan et al. (2010) found that the corrections to the absolute brightness of the supernovae were more dependent on metallicity than on stellar mass. However, the metallicities studied were calculated using a mass-metallicity relation in which more massive galaxies had higher metallicities, so there is some degeneracy to consider in the effects of stellar mass and metallicity. Mass-independent measures of metallicity would help separate the effect of metallicity from that of mass. Howell et al. (2009) found a correlation between the luminosity-weighted age of the host galaxy and the SN ^{5}6Ni yield, such that more massive progenitors had brighter explosions. As more massive stars are found in regions of active star formation, younger stellar populations can be expected to have more luminous SNe. Sullivan et al. (2010) also found that SNe in massive galaxies with low specific star formation rates have brigher luminosities.

Several of the host galaxy properties discussed above correlate with the stellar mass, or depend on the stellar mass. Corrections to the SN light curves based on their host galaxy

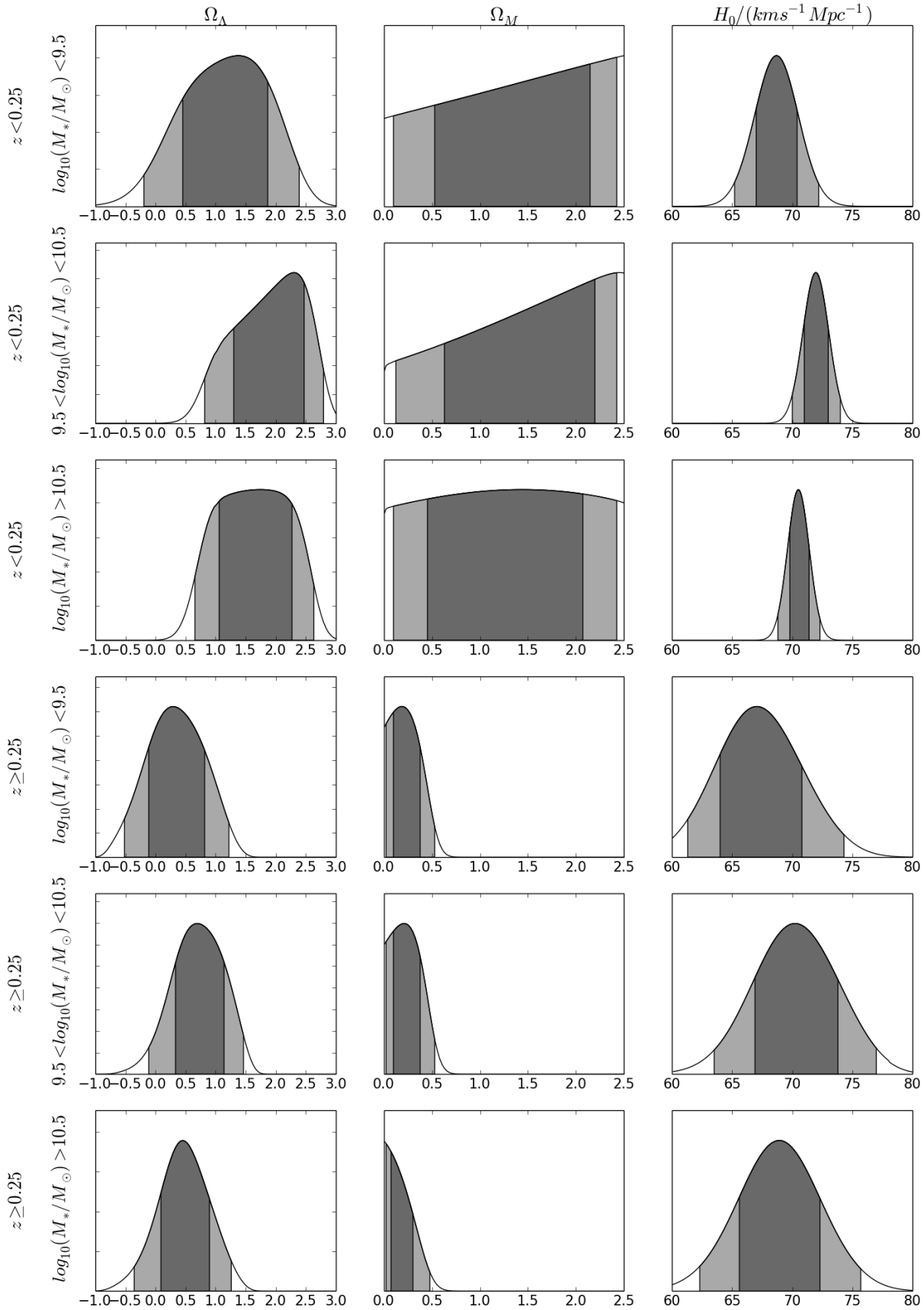

Figure 5. Cosmological parameters from every subsample in redshift-mass space. The shaded intervals represent the 1-and 2-σ confidence intervals (68.3% and 95.4%) as calculated from the normalized cumulative density functions. Note these distributions are highly non-Gaussian, however.

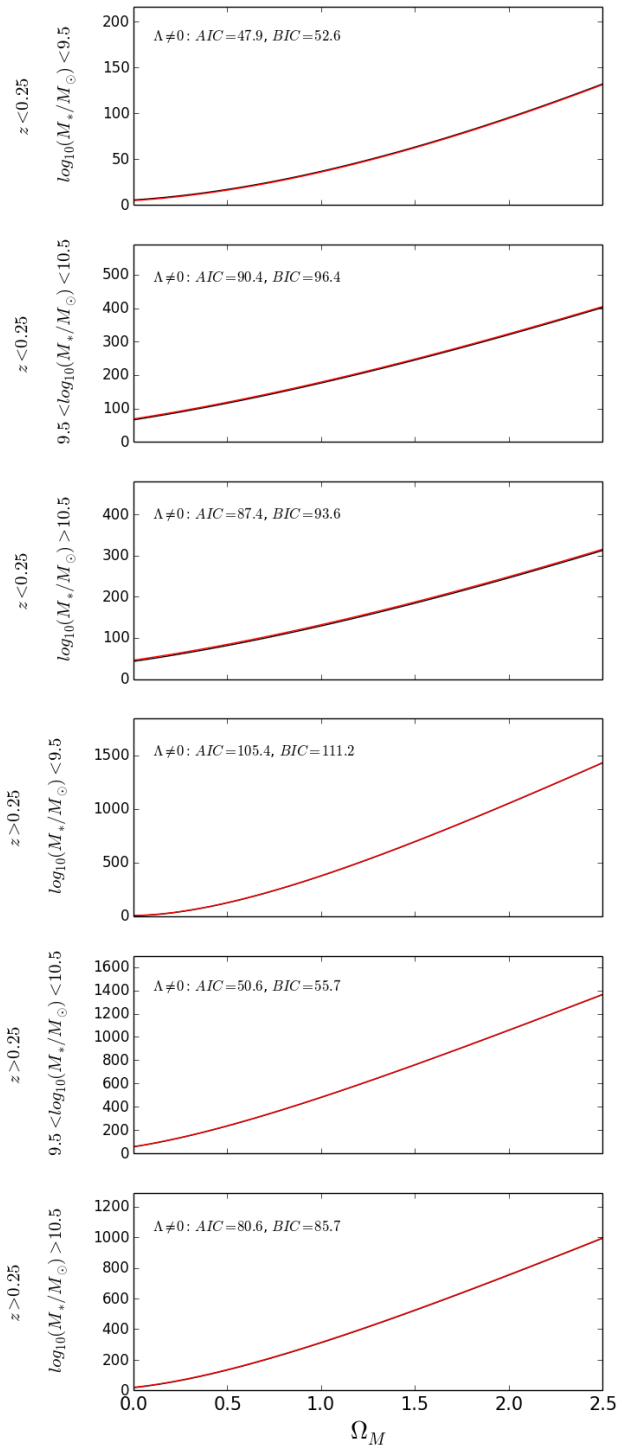

Figure 6. Comparison of data fits to model universes with and without the cosmological constant, using the Akaike Information Criterion. The lines indicate ΔAIC (black) and ΔBIC (red), calculated from slices in AIC or BIC $\Omega_\Lambda - \Omega_M$ space corresponding to $\Lambda = 0$. The numbers in the top left of each plot give the AIC and BIC values for the best-fit universe for that $z-M$ subsample without having constrained Ω_Λ

stellar mass then, on average, account for the host galaxy environment. More work could be done to study the effect of different host galaxy properties, considered independently of stellar mass, to make sure that the environment is fully considered and corrected for when computing distances and cosmological parameters.

It would be remiss not to add that, should host galaxy properties be better characterized, it will be more feasible to put stronger constraints on the identity of SNe Ia progenitors. The $z-M$ subsamples that we consider here are too coarse for such a task, but a similar study that includes many more parameters could point a clearer path to different production channels.

6. SUMMARY

In this paper, we used the sample and methodology of Betoule, M. et al. (2014) to determine cosmological parameters, Ω_M and Ω_Λ, and the effect of redshift and host galaxy environment on the cosmological model obtained. We used stellar mass as a proxy for host galaxy environment. Our sample of 740 SNe Ia was divided into six redshift-host galaxy stellar mass subsamples, with a redshift cut at $z = 0.25$ and stellar mass cuts at $\log_{10} M_\star/M_\odot = 9.5$ and 10.5.

The determined cosmological parameters, Ω_M, Ω_Λ, and H_0, for each subsample are listed in Table 2. We find that Ω_M and Ω_Λ are much better constrained by the high-redshift samples than the low-redshift samples. The probability distributions of Ω_M and Ω_Λ depend on the value of H_0 used. Samples with different host galaxy stellar masses yield slightly different results; this may be due to an incomplete correction for host galaxy properties on the light curves. We also calculated the AIC and BIC test criteria for our models compared to a $\Omega_\Lambda = 0$ universe, and found that, for all six redshift-stellar mass subsamples, a $\Omega_\Lambda \neq 0$ model is strongly preferred.

Future work regarding host galaxy properties' effect on SN light curves may involve consideration of other host galaxy parameters and fitting for corrections due to host galaxy parameters alongside cosmological parameters. Additional work would involve a joint analysis of the low-z and high-z samples.

We thank Dmitrios Psaltis for his guidance and knowledge in the use of different statistical methods in astronomy. We also thank Ekta Patel for insightful and enlivening discussions.

REFERENCES

Akaike, H. 1974, Automatic Control, IEEE Trans, 19, 716
Alam, S., Albareti, F. D., Prieto, C. A., et al. 2015, ApJ Supp Ser, 219, 12
Altavilla, G., Fiorentino, G., Marconi, M., et al. 2004, MNRAS, 349, 1344
Astier, P., Guy, J., Regnault, N., et al. 2006, A&A, 447, 31
Astier, P., El Hage, P., Guy, J., et al. 2013, A&A, 557, A55
Balland, C., Baumont, S., Basa, S., et al. 2009, A&A, 507, 85
Benetti, S., Meikle, P., Stehle, M., et al. 2004, MNRAS, 348, 261
Betoule, M., Marriner, J., Regnault, N., et al. 2013, A&A, 552, A124
Betoule, M., Kessler, R., Guy, J., et al. 2014, A&A, 568, A22
Bronder, T., Hook, I., Astier, P., et al. 2008, A&A, 477, 717
Carroll, S. M., Press, W. H., & Turner, E. L. 1992, ARA&A, 30, 499
Conley, A., Guy, J., Sullivan, M., et al. 2011, ApJS, 192, 1
Ellis, R. S., Sullivan, M., Nugent, P., et al. 2008, ApJ, 674, 51
Frieman, J. A., Turner, M. S., & Huterer, D. 2008, ARAA, 46, 385
Frieman, J. A., Bassett, B., Becker, A., et al. 2007, AJ, 135, 338
Guy, J., Sullivan, M., Conley, A., et al. 2010, A&A, 523, A7
Hamuy, M., Phillips, M. M., Maza, J., et al. 1995, AJ, 109, 1
Hamuy, M., Phillips, M. M., Suntzeff, N. B., et al. 1996, AJ, 112, 2391
Hamuy, M., Maza, J., Pinto, P. A., et al. 2002, AJ, 124, 417
Hicken, M., Challis, P., Jha, S., et al. 2009, ApJ, 700, 331
Holtzman, J. A., Marriner, J., Kessler, R., et al. 2008, AJ, 136, 2306
Howell, D. A., Sullivan, M., Brown, E. F., et al. 2009, ApJ, 691, 661
Jha, S., Kirshner, R. P., Challis, P., et al. 2006, AJ, 131, 527
Jiménez, N., Tissera, P. B., & Matteucci, F. 2015, ApJ, 810, 137
Johansson, J., Thomas, D., Pforr, J., et al. 2013, MNRAS, 435, 1680
Landolt, A. U. 1992, AJ, 104, 340
Landolt, A. U., & Uomoto, A. K. 2007, AJ, 133, 768
Leibundgut, B. 2001, ARAA, 39, 67
Maoz, D., Mannucci, F., & Nelemans, G. 2014, ARAA, 52, 107
Matheson, T., Kirshner, R. P., Challis, P., et al. 2008, AJ, 135, 1598
Park, C., Choi, Y.-Y., Kim, J., et al. 2012, ApJ L, 759, L7

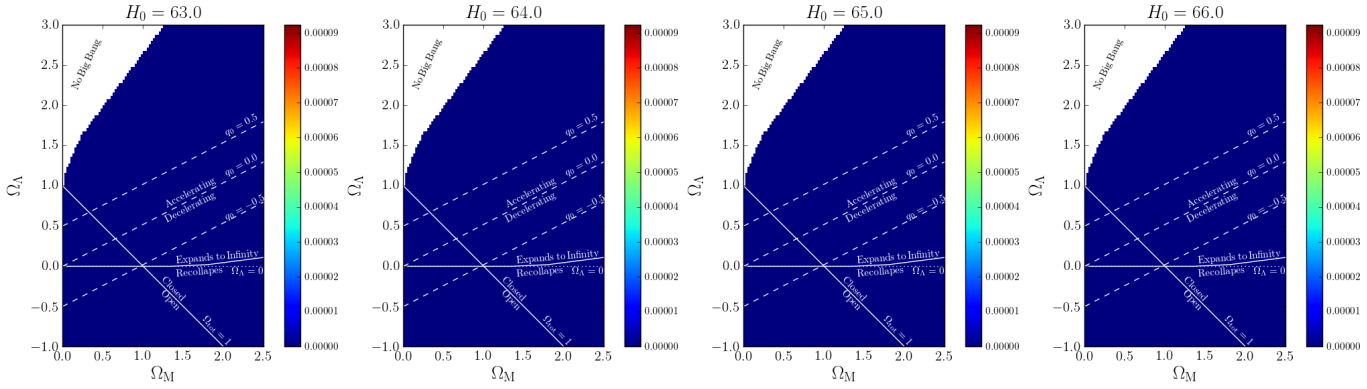

(a) $H_0 = 63.0\,\mathrm{Mpc\,km^{-1}\,s}$ (b) $H_0 = 64.0\,\mathrm{Mpc\,km^{-1}\,s}$ (c) $H_0 = 65.0\,\mathrm{Mpc\,km^{-1}\,s}$ (d) $H_0 = 66.0\,\mathrm{Mpc\,km^{-1}\,s}$

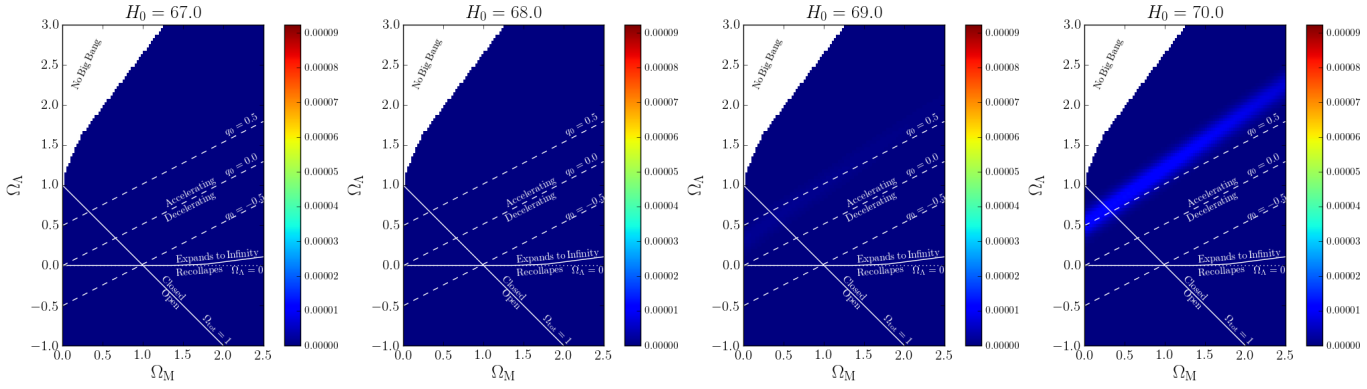

(e) $H_0 = 67.0\,\mathrm{Mpc\,km^{-1}\,s}$ (f) $H_0 = 68.0\,\mathrm{Mpc\,km^{-1}\,s}$ (g) $H_0 = 69.0\,\mathrm{Mpc\,km^{-1}\,s}$ (h) $H_0 = 70.0\,\mathrm{Mpc\,km^{-1}\,s}$

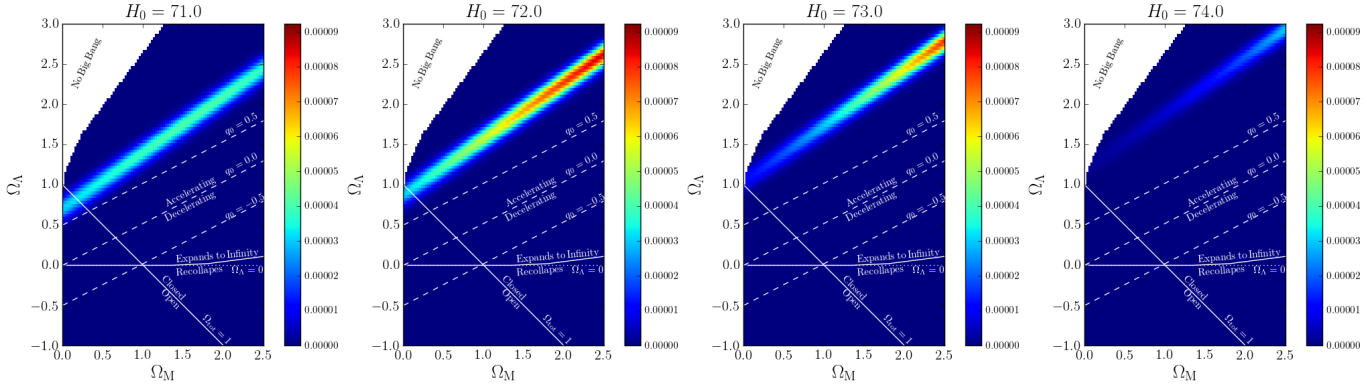

(i) $H_0 = 71.0\,\mathrm{Mpc\,km^{-1}\,s}$ (j) $H_0 = 72.0\,\mathrm{Mpc\,km^{-1}\,s}$ (k) $H_0 = 73.0\,\mathrm{Mpc\,km^{-1}\,s}$ (l) $H_0 = 74.0\,\mathrm{Mpc\,km^{-1}\,s}$

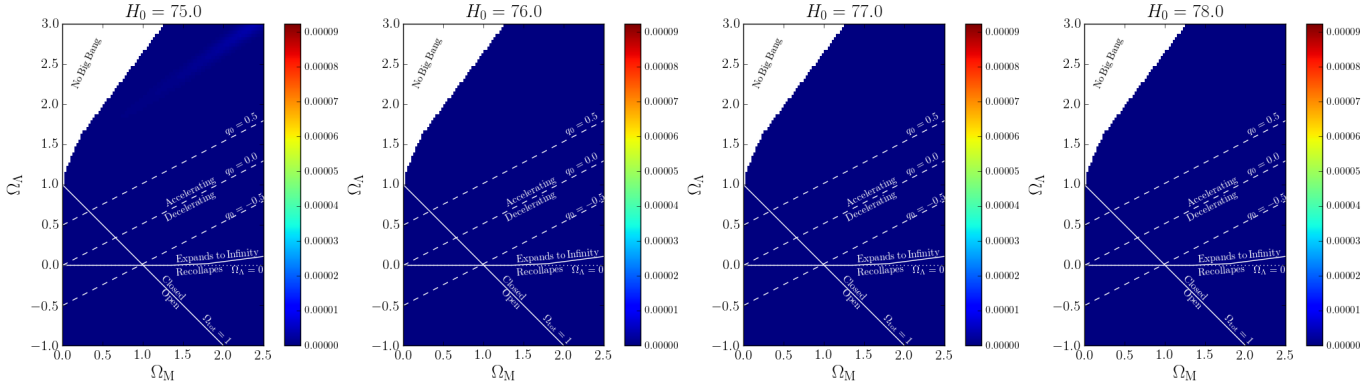

(m) $H_0 = 75.0\,\mathrm{Mpc\,km^{-1}\,s}$ (n) $H_0 = 76.0\,\mathrm{Mpc\,km^{-1}\,s}$ (o) $H_0 = 77.0\,\mathrm{Mpc\,km^{-1}\,s}$ (p) $H_0 = 78.0\,\mathrm{Mpc\,km^{-1}\,s}$

Figure 7. The probability density function of low-redshift supernovae ($z \leq 0.25$) with mid-host galaxy stellar mass ($10^{9.5} < M_* \leq 10^{10.5}$) for ($\Omega_M$, Ω_Λ) in each integer values of H_0 considered between $63.0 \leq H_0 \leq 78.0\,\mathrm{Mpc \cdot km^{-1}\,s}$.

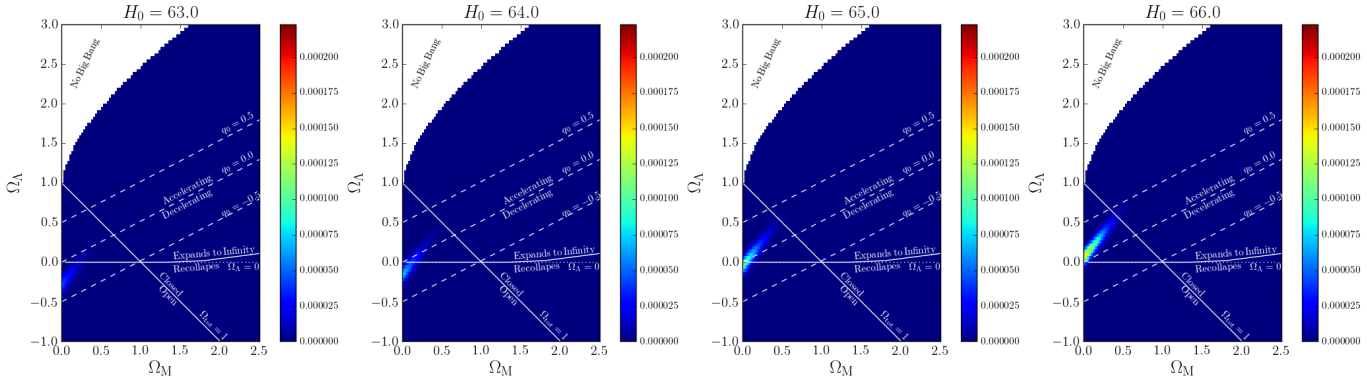

(a) $H_0 = 63.0\,\mathrm{Mpc\,km^{-1}\,s}$ (b) $H_0 = 64.0\,\mathrm{Mpc\,km^{-1}\,s}$ (c) $H_0 = 65.0\,\mathrm{Mpc\,km^{-1}\,s}$ (d) $H_0 = 66.0\,\mathrm{Mpc\,km^{-1}\,s}$

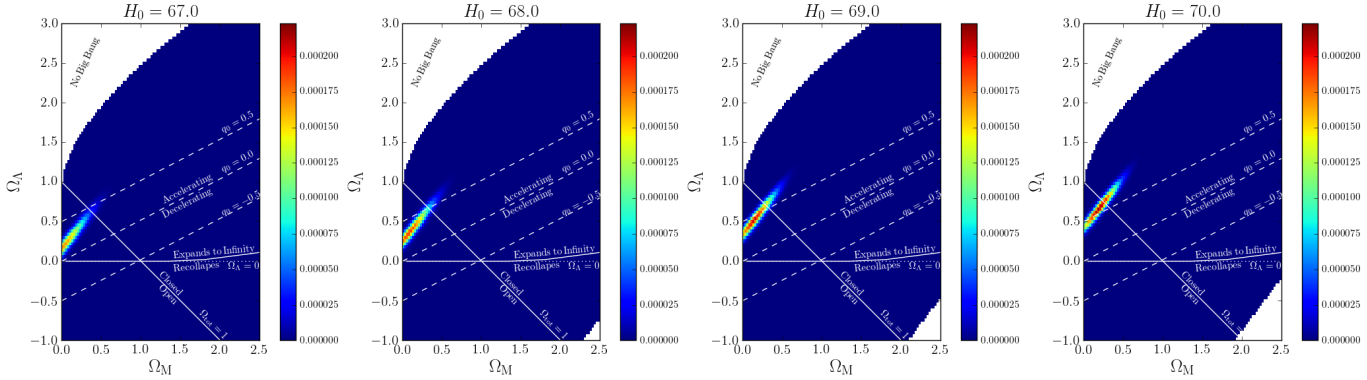

(e) $H_0 = 67.0\,\mathrm{Mpc\,km^{-1}\,s}$ (f) $H_0 = 68.0\,\mathrm{Mpc\,km^{-1}\,s}$ (g) $H_0 = 69.0\,\mathrm{Mpc\,km^{-1}\,s}$ (h) $H_0 = 70.0\,\mathrm{Mpc\,km^{-1}\,s}$

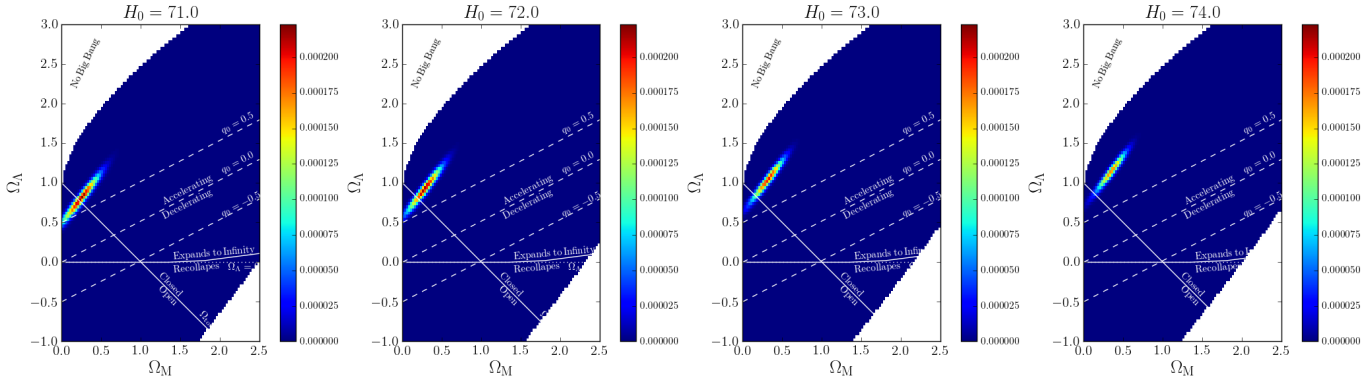

(i) $H_0 = 71.0\,\mathrm{Mpc\,km^{-1}\,s}$ (j) $H_0 = 72.0\,\mathrm{Mpc\,km^{-1}\,s}$ (k) $H_0 = 73.0\,\mathrm{Mpc\,km^{-1}\,s}$ (l) $H_0 = 74.0\,\mathrm{Mpc\,km^{-1}\,s}$

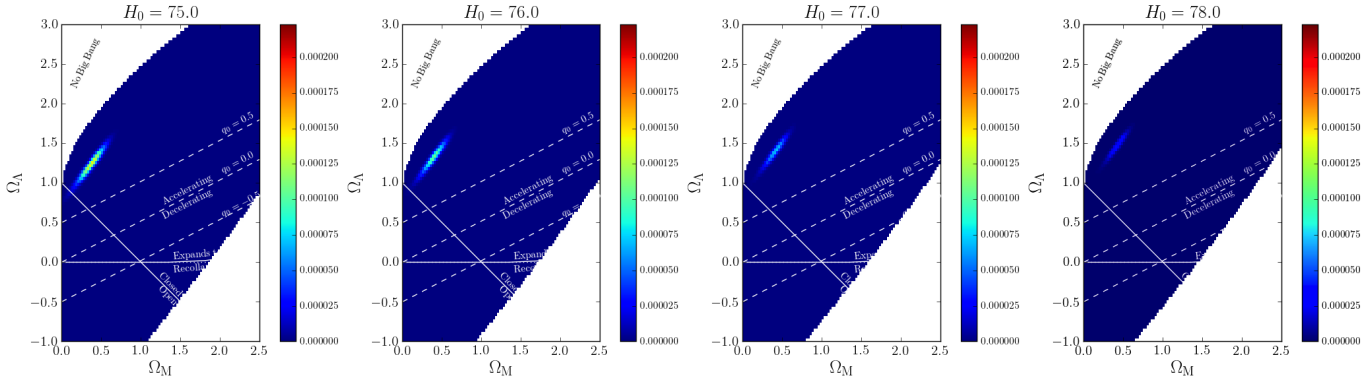

(m) $H_0 = 75.0\,\mathrm{Mpc\,km^{-1}\,s}$ (n) $H_0 = 76.0\,\mathrm{Mpc\,km^{-1}\,s}$ (o) $H_0 = 77.0\,\mathrm{Mpc\,km^{-1}\,s}$ (p) $H_0 = 78.0\,\mathrm{Mpc\,km^{-1}\,s}$

Figure 8. The probability density function of high-redshift supernovae ($z > 0.25$) with mid-host galaxy stellar mass ($10^{9.5} < M_* \leq 10^{10.5}$) for ($\Omega_M$, Ω_Λ) in each integer values of H_0 considered between $63.0 \leq H_0 \leq 78.0\,\mathrm{Mpc \cdot km^{-1}\,s}$.

Patat, F., Benetti, S., Cappellaro, E., et al. 1996, MNRAS, 278, 111
Perlmutter, S., Aldering, G., Goldhaber, G., et al. 1999, ApJ, 517, 565
Phillips, M. M. 1993, ApJL, 413, L105
Pritchet, C. J., Howell, D. A., & Sullivan, M. 2008, ApJL, 683, L25
Riess, A. G., Filippenko, A. V., Challis, P., et al. 1998, AJ, 116, 1009
Riess, A. G., Kirshner, R. P., Schmidt, B. P., et al. 1999, AJ, 117, 707
Sako, M., Bassett, B., Becker, A., et al. 2007, AJ, 135, 348
Sako, M., Bassett, B., Becker, A. C., et al. 2014, arXiv preprint arXiv:1401.3317
Schmidt, B. P., Kirshner, R. P., Leibundgut, B., et al. 1994, ApJL, 434, L19
Schwarz, G., et al. 1978, The Annals of Statistics, 6, 461
Smith, C., Rest, A., Hiriart, R., et al. 2002, in Proc. SPIE, Vol. 4836, Survey and Other Telescope Technologies and Discoveries, ed. J. A. Tyson & S. Wolff, 395
Smith, M., Nichol, R. C., Dilday, B., et al. 2012, ApJ, 755, 61
Sullivan, M., Howell, D. A., Perrett, K., et al. 2006, AJ, 131, 960
Sullivan, M., Conley, A., Howell, D., et al. 2010, MNRAS, 406, 782
Sullivan, M., Guy, J., Conley, A., et al. 2011, ApJ, 737, 102
Tripp, R. 1998, A&A, 331, 815
Wright, E. L. 2006, PASP, 118, 1711
York, D. G., Adelman, J., John E. Anderson, J., et al. 2000, AJ, 120, 1579

APPENDIX

COSMOLOGICAL PARAMETERS

The following is a condensed summary of the procedure in Sec. 4.1 of Riess et al. (1998), which we have followed to calculate the probability of the data fit to cosmological models. Equation numbers in Riess et al. (1998) are indicated with an 'R'.

Given the theoretical and measured distance moduli, we can calculate the χ^2 across parameter space as Eqn. (R4)

$$\chi^2(H_0,\Omega_M,\Omega_\Lambda)=\sum_i \frac{[\mu_{p,i}(z_i|H_0,\Omega_M,\Omega_\Lambda)-\mu_{0,i}]^2}{\sigma^2_{\mu 0,i}+\sigma^2_v}, \tag{A1}$$

where the subscript p denotes predicted values. (In our analysis, we considered σ_v to be zero because the dataset did not have that information.) Bayes' theorem implies the following expression for the probability of cosmological parameters, given the empirical distance moduli (Eqn. R5):

$$p(H_0,\Omega_M,\Omega_\Lambda|\{\mu_0\})=\frac{p(\{\mu_0\}|H_0,\Omega_M,\Omega_\Lambda)p(H_0,\Omega_M,\Omega_\Lambda)}{p(\{\mu_0\})}. \tag{A2}$$

where the priors are considered to be flat, and their ratio need not be calculated independently, because they can be recovered in the normalization process. The distance moduli are assumed to be independent and to have Gaussian errors, yielding the following likelihood function (Eqn. R7)

$$p(\{\mu_0\}|H_0,\Omega_M,\Omega_\Lambda)=\prod_i \frac{1}{\sqrt{2\pi(\sigma^2_{\mu 0,i}+\sigma^2_v)}}\exp\left\{-\frac{[\mu_{p,i}(z_i|H_0,\Omega_M,\Omega_\Lambda)-\mu_{0,i}]^2}{2(\sigma^2_{\mu 0,i}+\sigma^2_v)}\right\}. \tag{A3}$$

where the χ^2 clearly appears in the exponent. Normalizing, we have Eqn. (R10),

$$p(H_0,\Omega_M,\Omega_\Lambda|\{\mu_0\})=\frac{e^{-\chi^2/2}}{\int_{-\infty}^{\infty}dH_0\int_{-\infty}^{\infty}d\Omega_\Lambda\int_0^{\infty}\exp(-\chi^2/2)d\Omega_M} \tag{A4}$$

The probability density functions of any of the parameters H_0, Ω_M, or Ω_Λ are recovered by marginalizing the above expression over the other two 'nuisance' parameters.

We expect most of the probability in the likelihood probability density function will be in the vicinity of the peak. Moreover, in the vicinity of the peak of the likelihood function, we can approximate the density as a multivariate Gaussian. This is equivalent to looking only at the second-order terms in the Taylor expansion of the log-likelihood function. Defining the parameter vector $\vec{l}$, we can rewrite the likelihood as

$$\vec{l}\equiv[H_0 \quad \Omega_M \quad \Omega_\Lambda]^T \tag{A5}$$

The Gaussian approximation about the best-fit location $\hat{z}$ is then

$$p(\{\mu_0\}|\vec{l}) \propto p(\{\mu_0\}|\hat{l}) \exp\left[-\frac{1}{2}(\vec{l}-\hat{l})^T C^{-1}(\vec{l}-\hat{l})\right] \tag{A6a}$$

$$\propto \exp\left[\frac{1}{2}\chi^2\right] \exp\left[-\frac{1}{2}(\vec{l}-\hat{l})^T C^{-1}(\vec{l}-\hat{l})\right] \tag{A6b}$$